CrossMark

Theoretical and Experimental Study on Thermoelectric Properties of $Ba_8TM_xGa_yGe_{46-x-y}$ (TM = Zn, Cu, Ag) Type I Clathrates

JULIUSZ LESZCZYNSKI,[1,3,4] ANDRZEJ KOLEZYNSKI,[1] JAROSłAW JURASZEK,[2] and KRZYSZTOF WOJCIECHOWSKI[1]

1.—Faculty of Materials Science and Ceramics, AGH University of Science and Technology, Al. A. Mickiewicza 30, 30-059 Kraków, Poland. 2.—*Present address:* Polish Academy of Sciences, Institute of Low Temperature and Structure Research, Wrocław, Poland. 3.—e-mail: jleszczy@ agh.edu.pl. 4.—e-mail: Juliusz.Leszczynski@agh.edu.pl

In the type I clathrates $Ba_8TM_xGa_yGe_{46-x-y}$ (TM = group 10 to 12 elements) where some of the Ge framework atoms are substituted by Zn, Cu or Ag, the transition-metal elements prefer to occupy the $6c$ site. Preliminary band-structure calculations showed that this substitution implies modification of the electronic bands in the vicinity of the energy gap. By appropriate tailoring of the band structure, improved thermoelectric properties can be obtained. More detailed full-potential linearized augmented plane wave (FP-LAPW) method calculations within density functional theory (DFT) were performed using the WIEN2k package for compositions where the transition element TM fully occupies the $6c$ site. Additional analysis of the properties of the electron density topology within Bader's atoms-in-molecules approach was carried out to study the chemical bonding in intermetallic clathrates. To verify the theoretical predictions, polycrystalline samples of the type I clathrates Ba_8TM_x Ga_yGe_{46-x-y} (TM = Zn, Cu, Ag) modified by transition-metal element substitution for Ge were obtained. The samples were characterized using powder x-ray diffraction analysis, scanning electron microscopy, and energy-dispersive x-ray spectroscopy. The electrical conductivity, Seebeck coefficient, and thermal conductivity were measured in the temperature range from 320 K to 720 K. Several models were used to fit the experimental results for the electronic transport properties and to estimate the energy gap. Vacancies at the Ge site were considered responsible for deviations from the desired properties, and appropriate defect equations correlating the vacancies and TM concentration are presented. Finally, the results of DFT calculations are compared with the experiments, showing good agreement with theoretically predicted cell parameters and general observations of the transport properties.

Key words: Germanium clathrate, thermoelectric materials, thermal conductivity, band structure, WIEN2k, DFT calculations

INTRODUCTION

In the quest for better thermoelectric materials, the attention of researchers has focused on so-called cage compounds.[1–3] The particular feature of these compounds is the presence of large structural voids in their structure, which can be filled with "guest" atoms. The distance between such "guests" and neighboring atoms is greater compared with, e.g., binary compounds of the two elements, thus they form weaker bonds and allow for large vibrations of the guest atoms. This effect can be observed as

Theoretical and Experimental Study on Thermoelectric Properties of $Ba_8TM_xGa_yGe_{46-x-y}$
(TM = Zn, Cu, Ag) Type I Clathrates

5265

an increased temperature dependence of the atomic displacement parameter (ADP) of the guest atoms.[1] The most interesting result of this feature is very low thermal conductivity in many such cage compounds. Many theories have been used to explain this behavior, the most popular and illustrative being "rattling" of guest atoms, where loosely bonded atoms are regarded as Einstein oscillators acting as phonon scattering centers.[1] However, more recent inelastic neutron scattering experiments and Raman spectroscopy measurements point to different mechanisms for the reduced thermal conductivity of type I clathrates and refute the scenario of guest atoms as independent oscillators.[4] A comprehensive overview of the current state of knowledge on glass-like thermal conductivity in clathrates is given by Takanabe et al.[5] Due to their particular transport properties, germanium clathrates with type I structure are a group of promising thermoelectric materials. Their structure can be described as a combination of two types of germanium polyhedra, namely two small dodecahedra and six larger tetrakaidecahedra, per unit cell (Fig. 1). The structural cages are symmetrically arranged, forming a cubic structure in space group $Pm\bar{3}n$, and can be occupied by strongly electropositive elements from group 1 and 2 of the Periodic Table. The bonding between guest and host atoms is mainly ionic, and the negative charge of the guests is transferred to the framework atoms. In the case of germanium clathrates, to reach thermodynamic stability of such structure, most of this charge must be compensated by substitution of germanium for elements with fewer valence electrons, e.g., gallium or zinc, or by formation of Ge vacancies. As a result of chemical and geometrical inequivalences, when substituting the group 14 framework atoms by other elements, some rules for site occupation preferences can be formulated and are reflected in experimental observations.[4] For the anionic Ge clathrates $Ba_8M_xGe_{46-x}$, substitution by M atoms with fewer valence electrons takes place preferentially at 6c site. The same site is preferred for vacancy formation. In the case of transition-metal elements from groups 10 to 12, they can occupy only the 6c site for $x < 6$,[7] while for $x > 6$ the 6c site and partly the 16i site.[8]

The results of electronic structure calculations for several TM-substituted clathrates have already been presented,[9–11] but they were limited to only density-of-states functions and band structure. In the present study, we investigated the band structure of Ba–Ge type I clathrates with selected compositions modified by substitution of Zn, Cu, Ag, and Ga, as well as the impact of such substitution on the bond properties, band dispersion, and relative positions of bands, and we compare with electronic transport measurements.
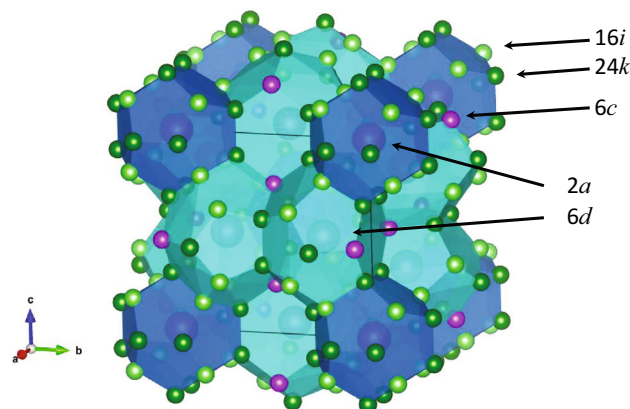

Fig. 1. Crystal structure of type I Ge clathrates.[6]

COMPUTATIONAL DETAILS

Band-structure and density-of-states calculations for $Ba_8Ga_6Ge_{40}$, $Ba_8Zn_6Ge_{40}$, $Ba_8Zn_3Cu_3Ge_{40}$, $Ba_8Cu_6Ge_{40}$, and $Ba_8Ag_6Ge_{40}$ have been performed using the WIEN2k full-potential linearized augmented plane wave (FP-LAPW) *ab initio* package[12] within the density functional theory (DFT) formalism.[13–17] For the calculations, 500 **k**-points ($7 \times 7 \times 7$ mesh with 20 **k** points in the irreducible Brillouin zone), cutoff parameter $Rk_{max} = 7.5$, and generalized gradient approximation Perdew–Burke–Ernzerhof (GGA-PBE) exchange–correlation potential were chosen. For more accurate evaluation of the energy bandgap, the modified Becke–Johnson exchange–correlation potential was used for density-of-states (DOS) computations.[18] The muffin-tin radius (R_i) [a.u.] was set to 2.5 for Ba, 2.29 for Ga, and 2.35 for Ge. The convergence criteria for self-consistent field (SCF) method calculations were chosen as $\Delta E_{SCF} = 10^{-5}$ Ry for total energy and $\Delta\rho_{SCF} = 10^{-5}$ e for electron density topology analysis. As initial data, the cell parameters and fractional atomic coordinates were taken from Rietveld crystal structure refinement for $Ba_8Ga_{16}Ge_{30}$ and $Ba_8TM_xGa_yGe_{40-x-y}$ (TM = Zn, Cu, Ag), then all structures were fully optimized (cell parameters and atomic positions). For $Ba_8Ga_6Ge_{40}$, a virtual crystal (VC) model was used, where the 6c and 16i sites were occupied by Ge and the 24k site by an artificial atom with atomic number $Z = 31.75$ ($Ga_{6/24}Ge_{18/24}$). This model was selected to study the impact of Ge substitution by Ga at different sites on the band structure of the clathrates, as in our previous work we have already calculated the electronic structure of $Ba_8Ga_6Ge_{40}$ with Ga occupying the 6c position. For the other compositions, i.e., $Ba_8Zn_6Ge_{40}$, $Ba_8Zn_3Cu_3Ge_{40}$, $Ba_8Cu_6Ge_{40}$, and $Ba_8Ag_6Ge_{40}$, Zn, Cu, Ag, and an artificial atom $Cu_{1/2}Zn_{1/2}$ with $Z = 29.5$ were assumed to fully occupy the 6c position. Additional analysis of the electron density topology properties

within Bader's atoms-in-molecules approach was carried out for $Ba_8Ga_6Ge_{40}$, $Ba_8Zn_6Ge_{40}$, $Ba_8Cu_3Zn_3Ge_{40}$, $Ba_8Cu_6Ge_{40}$, and $Ba_8Ag_6Ge_{40}$.

EXPERIMENTAL PROCEDURES

Four series of $Ba_8TM_yGa_zGe_{46-x-y-z}$ samples were prepared containing different TMs: (a) Zn, (b) $Cu_{1/2}Zn_{1/2}$, (c) Cu, and (d) Ag. Each series consisted of three samples with nominal compositions $Ba_8Zn_6Ga_xGe_{40-x}$ ($x = 3, 4, 5$), $Ba_8Zn_3Cu_3Ga_xGe_{40-x}$ ($x = 0, 1, 2$), $Ba_8Cu_5Ga_xGe_{41-x}$ ($x = 0, 1, 2$), and $Ba_8Ag_5Ga_xGe_{41-x}$ ($x = 0, 1, 2$), corresponding to different nominal numbers of excess electrons per unit cell (u.c.): (i) 1 e/u.c, (ii) 0 excess e/u.c. (a completely charge-balanced sample), and (iii) −1 e/u.c. (one-electron-deficient sample). The nominal number of excess electrons was obtained from a simple electron-counting scheme. All specimens were prepared by melting and crystallization of stoichiometric amounts of Ga, Zn, Cu, Ag, and Ge with 5 wt.% excess Ba used to compensate Ba loss during synthesis. The mixed reactants were placed in an alumina crucible and closed in a stainless-steel container filled with Ar and sealed by welding. After melting at 1320 K for 30 min, specimens were annealed at 1170 K for 72 h. Obtained ingots were ground into powder. Finally, the specimens were densified using the spark plasma sintering/field-assisted sintering technology (SPS/FAST) method at 1120 K to 1170 K for 15 min under pressure of 50 MPa in Ar atmosphere. More details can be found in our earlier publication.[19] The microstructure and chemical composition of the obtained specimens were examined by scanning electron microscopy (SEM; JEOL JSM-840) and energy-dispersive x-ray spectroscopy (EDS, EDAX), respectively. The phase composition and structural parameters were analyzed by the powder x-ray diffraction (PXRD) method using a PANalytical Empyrean diffractometer with unfiltered Cu K_α radiation. Measurements of electronic transport properties as well as thermal conductivity are described in detail elsewhere.[19] All of the nominally one-electron-deficient samples exhibited n-type instead of p-type conductivity, and the Seebeck coefficient, resistivity, and thermal conductivity results for these samples are not presented. Synthesis of p-type material is a known issue for type I clathrates in the Ba–Ge system.

RESULTS AND DISCUSSION

Electronic Structure Calculations

The electronic band structures were calculated for the following compositions: $Ba_8Ga_6Ge_{40}$, $Ba_8Zn_6Ge_{40}$, $Ba_8Cu_3Zn_3Ge_{40}$, $Ba_8Cu_6Ge_{40}$, and $Ba_8Ag_6Ge_{40}$. Plots of the calculated densities of states projected onto particular atoms are presented in Fig. 2. DOS calculations showed that $Ba_8Ga_6Ge_{40}$, $Ba_8Zn_6Ge_{40}$, and $Ba_8Cu_3Zn_3Ge_{40}$ are

strongly degenerate n-type semiconductors, while $Ba_8Cu_6Ge_{40}$ and $Ba_8Ag_6Ge_{40}$ are degenerate p-type semiconductors. These results are in agreement with the Zintl–Klemm concept, which is often used to predict and explain electronic properties of clathrates. A charge-balanced structure of Ge type I clathrate contains $46Ge \times 4 = 184$ valence electrons per unit cell. Each Ba atom donates two excess electrons to the framework, while Ga, Zn, Cu, and Ag are, respectively, one, two, three, and three electron deficient. Counting valence electrons, we obtain 194, 188, 185, 182, and 182 electrons per formula unit for $Ba_8Ga_6Ge_{40}$, $Ba_8Zn_6Ge_{40}$, $Ba_8Cu_3Zn_3Ge_{40}$, $Ba_8Cu_6Ge_{40}$, and $Ba_8Ag_6Ge_{40}$, respectively. All of the calculated band structures except that for $Ba_8Ga_6Ge_{40}$ are very similar. The different structural model with virtual $Ga_{6/24}Ge_{18/24}$ atom at the $24k$ site results in significant differences in the valence- and conduction-band shape and dispersion for $Ba_8Ga_6Ge_{40}$. However, the band structure of $Ba_8Ga_6Ge_{40}$ calculated in our previous study, where full occupation of $6c$ position by Ga was assumed, is very similar to those calculated for $Ba_8TM_6Ge_{40}$. The valence bands (VB) in all of the compounds are formed by strongly hybridized Zn, Cu, Ag, Ga, and Ge bonding orbitals with negligible participation of guest atom states. The main differences are observed for the densities of states of atoms at the $6c$ site (Fig. 2). In the case of $Ba_8Ga_6Ge_{40}$, mainly Ga and Ge s- and p-orbitals contribute to the valence band. For the remaining structures containing transition metal, mainly d-, p-, and s-states of Zn, Cu, and Ag, apart from the Ga and Ge s- and p-orbitals, are involved in formation of the valence band. The d-band has the lowest energy for Zn (−8 eV below the top of the VB), and its energy increases for the artificial atom $Cu_{1/2}Zn_{1/2}$ and for Ag, reaching the highest value for Cu. The top edge of the valence band, which is interesting from the electronic transport perspective, consists of the $16i$- and $24d$-site Ge and Ga p-orbitals for all the studied cases, and the contribution from the $6c$ site depends strongly on the atom type. In the case of Ge and Ga at the $6c$ site, mainly p- and s-orbitals form the top of the band. Zn is an intermediate case where the band consists mainly of p-states but with an important contribution of d-states. For the artificial atom $Cu_{1/2}Zn_{1/2}$, the participation of d-states becomes equal to that of p-orbitals. For Cu and Ag, the d-character of these bands becomes dominant over the p-state character. The density of p-states decreases with decreasing energy down from the top of the VB. Simultaneously, the fraction of s-states in the DOS is increasing, and for energies 1.5 eV to 2 eV below the valence-band edge, this contribution exceeds that of the p-states. Comparing all of the studied atoms at the $6c$ site, the density of states of p- and s-orbitals remains similar but the contribution of d-states increases from Zn to Cu and Ag.

The conduction bands (CB) near the energy gap arise from the Ba($6d$) d-orbitals with some

Theoretical and Experimental Study on Thermoelectric Properties of $Ba_8TM_xGa_yGe_{46-x-y}$ (TM = Zn, Cu, Ag) Type I Clathrates
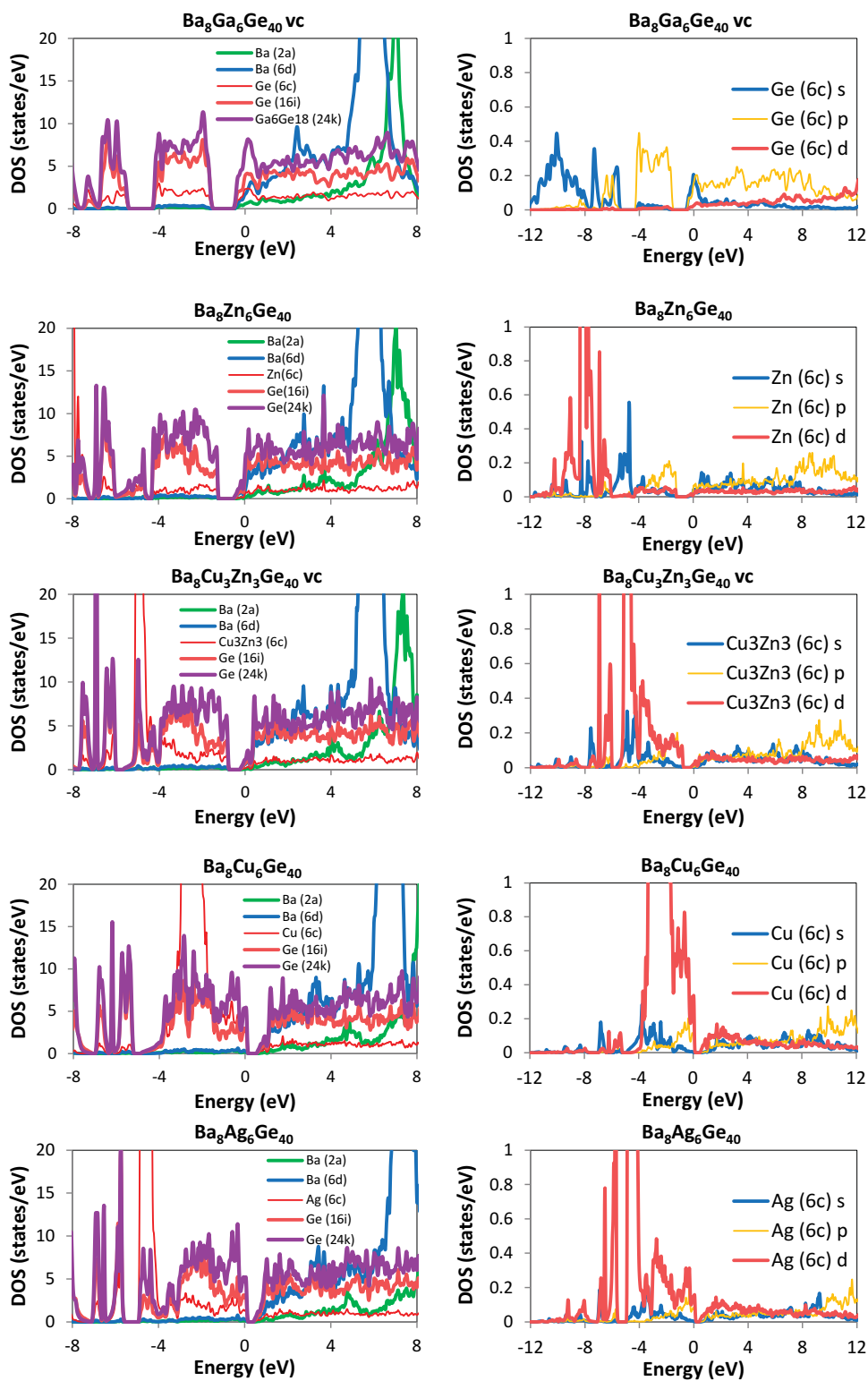
5267

Fig. 2. Total (left) and partial (right) electron density of states of calculated Ge clathrate structures.

participation of s-states just at the bottom of the CB, combined with antibonding states of the framework atoms mainly from the $16i$ and $24k$ sites. Ge bands have mainly hybrid sp character; as the energy increases, the contribution of s-orbitals decreases while that of d-orbitals increases. For TM, a similar

trend in the contribution of d-states to the DOS as described for the valence band is observed, and for Cu and Ag, purely d-orbitals are involved in the formation of the bands near the CB edge. However, change of the element at the $6c$ site has little impact on the overall electronic band structure, or on the total and partial DOS near the Fermi energy. The main change is a narrowing of the energy bandgap as the bands near the gap gain d-character. The calculated bandgaps for Ga, Zn, Cu$_{1/2}$Zn$_{1/2}$, Cu, and Ag clathrates are 0.76 eV, 0.63 eV, 0.44 eV, 0.33 eV, and 0.16 eV, respectively. Very similar results for calculated energy gaps can be found in literature.[9–11,20] However, those values are strongly dependent on the calculation method and thus difficult to compare. Our calculations show that the highest thermoelectric performance should be obtained for Ga- and Zn-substituted Ge clathrates, as they have the largest energy gaps and thus should have the lowest contribution from intrinsic carriers at high temperatures. The minor changes in the band structure validate the use of the virtual crystal approach in our calculations. These also show that use of the rigid-band approximation is correct for these compounds as long as the atom substitution refers to the same position. For samples with the same chemical composition but different site occupancy of the substituting element, the band structure and thus electronic properties will be different. As Ga also occupies sites other than $6c$, the band structure for Ba–Ga–Ge clathrates will be different from that for TM–Ge clathrates. Moreover, in the germanium clathrates, several structural changes are observed, depending on the type and concentration of element substituting for Ge, as well as the synthesis route. In several situations, splitting of the equilibrium positions of either the framework or guest atoms is observed.[8,21] Far deviation of the composition from charge balance towards excess electrons causes formation of framework atom vacancies, and at high vacancy concentrations, this leads to vacancy ordering with the formation of a superstructure.[22] Moreover, for a specific composition in the real material, different site occupancies are observed for different preparation methods, hence some dissimilarities of transport properties between different published data can be expected. All of these effects should be taken into account in band-structure calculations when appropriate, making reproduction of real material properties in a theoretical model quite complex.

For all of the calculated structures, the valence bands located close to the Fermi level have small dispersion, pointing to high effective mass of holes. The conduction bands near the gap are much steeper, resulting in lower effective mass of electrons, in agreement with literature data. The calculated lattice parameter follows quite well the change of the atomic radii of the substituting element, giving 11.0726 Å for Ga-, 10.9291 Å for Zn-, 10.8541 Å for Cu-, 10.8772 Å for Zn$_{0.5}$Cu$_{0.5}$-,

and 11.0065 Å for Ag-containing samples. These results correspond well with the trends observed experimentally in Ba–TM–Ge clathrates, but all of the lattice parameters are overestimated by about 0.9% compared with experimental values at 300 K: 10.7548 Å (Ba$_8$Zn$_6$Ge$_{40}$),[8] 10.6872 Å (Ba$_8$Cu$_6$Ge$_{40}$),[23] and 10.841 Å (Ba$_8$Ag$_{5.3}$Ge$_{40}$).[24] This difference is partly due to the fact that the computations were optimized toward energy gap calculation. It is also possible that point defects, mainly framework vacancies, may be the origin of this discrepancy. The lattice constant for Ba$_8$Zn$_6$Ge$_{40}$ of $a = 10.92$ Å calculated by Eto et al.[9] is in very good agreement with our result.

The results of analysis of the electron density topology by means of the quantum theory of atoms in molecules (QTAIM) are presented in Table I (for respective bond critical points) and Table II (for properties of topological atoms). The results for the composition with the virtual atom Cu$_{1/2}$Zn$_{1/2}$ are presented in the Electronic Supplementary Material (ESM), as they may be subject to computational artifacts resulting from the employed virtual crystal approximation, which is valid for electronic structure calculations but not necessarily for electron density topology analysis. One can see that, for all the structures, the bond critical point (BCP) properties are quite similar: Ba–Ge and TM–Ge bonds exhibit closed-shell-like properties (positive Laplacian, indicating charge depletion in bond critical point proximity), typical for ionic bonds, while Ge–Ge bonds are covalent (high electron density and negative Laplacian in BCP, indicating charge concentration in bond region). The net charge of Ba at $2a$ site is lower than for Ba($6d$) in the large cage, and it is much lower than the expected charge of +2 for a purely ionic-bond scenario. In the case of the $6d$ site, where the Ba–Ge distance is longer and thus overlapping of atomic orbitals is lower, Ba interactions with the cage-forming atoms are closer to ionic bond. The net charge of Ba at $6d$ position depends on the TM and increases with the electronegativity of the TM. However, this effect can also be linked to the degree of charge balance. The Ge–Ge bonds are clearly covalent, while the TM–Ge and Ga–Ge bonds have significant ionic character. As a consequence, contrary to the Ge framework atoms, Ga and Zn gain positive charge even for electron rich compositions according to the electronegativity difference between Ge and the corresponding atom. On the other hand, Cu and Ag, which have higher Pauling electronegativity values than Ga and Zn, but slightly lower and comparable to Ge (and generally much lower than Ge on other electronegativity scales), both have negative topological charge, for Ag exceeding the charge of Ge. Our results are similar to the findings of Baitinger et al.[25] ($q_{Zn} = +0.18$, $q_{Ga} = +0.17$, $q_{Cu} = -0.28$, $q_{Ag} = -0.35$), who studied a number of elements occupying the $6c$ site in Ba$_8$E$_6$Ge$_{30}$ using QTAIM. They showed that most transition metals from

Theoretical and Experimental Study on Thermoelectric Properties of $Ba_8TM_xGa_yGe_{46-x-y}$ (TM = Zn, Cu, Ag) Type I Clathrates

5269

Table I. Bond critical point (BCP) properties in $Ba_8Ga_6Ge_{40}$, $Ba_8Zn_6Ge_{40}$, $Ba_8Cu_3Zn_3Ge_{40}$, $Ba_8Cu_6Ge_{40}$, and $Ba_8Ag_6Ge_{40}$ crystal structures, calculated for FP-LAPW total electron density: electron density $\rho_{BCP}(r)$, Laplacian $\nabla^2\rho(\rho)$, and eigenvalues of Hessian matrix λ_1 to λ_3

	$\rho(r)$	$\nabla^2\rho(r)$	λ_1	λ_2	λ_3
$Ba_8Ga_6Ge_{40}$					
$r_{GaGe\text{-}Ba\ 6d}$	0.0100	0.0181	−0.0042	−0.0017	0.0240
$r_{GaGe\text{-}Ba\ 2a}$	0.0115	0.0231	−0.0030	−0.0016	0.0277
$r_{Ge\ 16i\text{-}Ba\ 2a}$	0.0130	0.0282	−0.0041	−0.0041	0.0365
$r_{GaGe\text{-}GaGe}$	0.0556	−0.0129	−0.0389	−0.0377	0.0637
$r_{GaGe\text{-}Ge\ 6c}$	0.0569	−0.0152	−0.0409	−0.0406	0.0663
$r_{GaGe\text{-}Ge\ 16i}$	0.0592	−0.0212	−0.0436	−0.0421	0.0645
$r_{Ge\ 16i\text{-}Ge\ 16i}$	0.0619	−0.0264	−0.0463	−0.0463	0.0663
$Ba_8Zn_6Ge_{40}$					
$r_{Ge\ 24k\text{-}Ba\ 6d}$	0.0102	0.0232	−0.0048	−0.0026	0.0306
$r_{Ge\ 24k\text{-}Ba\ 6d}$	0.0129	0.0287	−0.0033	−0.0031	0.0351
$r_{Ge\ 16i\text{-}Ba\ 2a}$	0.0134	0.0346	−0.0039	−0.0039	0.0425
$r_{Zn\text{-}Ge\ 24k}$	0.0499	0.0583	−0.0298	−0.0295	0.1176
$r_{Ge\ 24k\text{-}Ge\ 24k}$	0.0666	−0.0486	−0.0488	−0.0442	0.0444
$r_{Ge\ 24k\text{-}Ge\ 16i}$	0.0690	−0.0563	−0.0519	−0.0490	0.0445
$r_{Ge\ 16i\text{-}Ge\ 16i}$	0.0728	−0.0703	−0.0562	−0.0562	0.0421
$Ba_8Cu_3Zn_3Ge_{40}$					
$r_{Ge\ 24k\text{-}Ba\ 6d}$	0.0102	0.0222	−0.0046	−0.0024	0.0292
$r_{Ge\ 24k\text{-}Ba\ 6d}$	0.0124	0.0279	−0.0035	−0.0026	0.0340
$r_{Ge\ 16i\text{-}Ba\ 2a}$	0.0131	0.0330	−0.0039	−0.0039	0.0408
$r_{Cu1/2Zn1/2\text{-}Ge\ 24k}$	0.0507	0.0550	−0.0307	−0.0304	0.1160
$r_{Ge\ 24k\text{-}Ge\ 24k}$	0.0652	−0.0448	−0.0474	−0.0439	0.0465
$r_{Ge\ 24k\text{-}Ge\ 16i}$	0.0677	−0.0527	−0.0509	−0.0482	0.0465
$r_{Ge\ 16i\text{-}Ge\ 16i}$	0.0710	−0.0649	−0.0547	−0.0547	0.0444
$Ba_8Cu_6Ge_{40}$					
$r_{Ge\ 24k\text{-}Ba\ 6d}$	0.0107	0.0218	−0.0047	−0.0024	0.0289
$r_{Ge\ 24k\text{-}Ba\ 6d}$	0.0135	0.0270	−0.0032	−0.0030	0.0332
$r_{Ge\ 16i\text{-}Ba\ 2a}$	0.0144	0.0330	−0.0044	−0.0044	0.0417
$r_{Cu\text{-}Ge\ 24k}$	0.0492	0.0673	−0.029	−0.0281	0.1243
$r_{Ge\ 24k\text{-}Ge\ 24k}$	0.0630	−0.0256	−0.0462	−0.0431	0.0637
$r_{Ge\ 24k\text{-}Ge\ 16i}$	0.0649	−0.0312	−0.0488	−0.0468	0.0644
$r_{Ge\ 16i\text{-}Ge\ 16i}$	0.0678	−0.0412	−0.0522	−0.0522	0.0632
$Ba_8Ag_6Ge_{40}$					
$r_{Ge\ 24k\text{-}Ba\ 6d}$	0.0100	0.0199	−0.0043	−0.0021	0.0263
$r_{Ge\ 24k\text{-}Ba\ 6d}$	0.0125	0.0245	−0.0030	−0.0027	0.0302
$r_{Ge\ 16i\text{-}Ba\ 2a}$	0.0133	0.0300	−0.0039	−0.0039	0.0379
$r_{Ag\text{-}Ge\ 24k}$	0.0580	0.0249	−0.0409	−0.0406	0.1063
$r_{Ge\ 24k\text{-}Ge\ 24k}$	0.0600	−0.0200	−0.0436	−0.0407	0.0643
$r_{Ge\ 24k\text{-}Ge\ 16i}$	0.0618	−0.0250	−0.0461	−0.0443	0.0654
$r_{Ge\ 16i\text{-}Ge\ 16i}$	0.0643	−0.0335	−0.0490	−0.0490	0.0646

Table II. Results of electron density topology analysis: q atomic charge, Vol. atomic volume calculated for topological atoms

X $Ba_8X_6Ge_{40}$	Ba (2a)		Ba (6d)		X (6c)		Ge (16i)		Ge (24k)	
	q (e)	Vol. (Å^3)	q (e)	Vol. (Å^3)	q (e)	Vol. (Å^3)	q (e)	Vol. (Å^3)	q (e)	Vol. (Å^3)
Ga (6c)	1.21	167	1.27	200	0.10	134	−0.16	147	−0.33	156
Zn	1.18	170	1.36	207	0.14	130	−0.18	155	−0.35	165
Cu	1.16	167	1.40	202	−0.13	132	−0.17	152	−0.30	161
Ag	1.18	172	1.41	206	−0.42	170	−0.18	158	−0.23	161
$Ba_8Ga_{16}Ge_{40}$ Ga (24k)	1.17	177	1.34	212	−0.25	171	−0.23	165	−0.20	161
$Ba_8Ga_{16}Ge_{40}$ Ga (16i)	1.20	169	1.35	197	0.033	134	−0.18	154	−0.41	160

groups 10 to 13 exhibit negative topological charge in the type I Ge clathrate, which is connected with the electronegativity difference between Ge and TM. However, some of their results are somewhat different. The calculated net charge of Ba(6d) is smaller for each studied compound. For

$Ba_8Cu_6Ge_{30}$, the charge of Ba at both sites is higher than for $Ba_8Ag_6Ge_{30}$, while we found it to be almost equal. On the other hand, the charges of Cu and Ag in their findings are similar, while our results show three times higher negative charge for Ag. Much better quantitative agreement with our calculations can be found in Ref. 11 for the value of the Cu topological charge at 6c site: $q_{Cu} = -0.13e$.

If there is positive charge at TM, it may contribute to repulsive forces between neighboring TM atoms, and make direct TM–TM bonds energetically unfavorable. This can provide an additional explanation for the occupation of 6c site by the transition-metal atoms, as it is the only type I clathrate framework site at which atoms are isolated from other atoms at the same site. Moreover, the 6c site is a part of the large tetrakaidecahedral polyhedra where repulsion forces between the positively charged Ba and TM are lower. The positive net charge of TM may also explain difficulties in synthesis and stability of electron-deficient p-type clathrates. After reaching a certain positive charge, the repulsion between Ba and TM drives the framework to collapse and decompose the compound into TM-poorer clathrate and TM–Ge phase rich in TM. In the case of TM with strongly negative net charge (Au, Ni, Pt),[25] it is much easier to obtain p-type conductivity, possibly due to the contribution of electrostatic attraction forces to stabilization of the structure. Another explanation for the enhanced stability of some TM clathrates was given quite recently by Zhang et al.[26] and Baitinger et al.:[25] studying the electronic structure of selected clathrates using the electron localizability indicator ELI-D, they discovered additional interactions between Ba and Au and some other TM (Pd, Pt, Cd). Apart from the electrostatic interactions, steric and geometric factors also play a role in shaping the structure of clathrates. Neutron diffraction studies showed that, for n-type Ga-, Zn-, and Al-substituted Ge clathrates, the Ba in the tetrakaidecahedral cage occupies the off-center 24k site displaced toward the 6c framework sites, while for Ag, Au, and Cu (and p-type Ga), the Ba is moved from the central 6d site to the 24k site, but away from the 6c site. For Ga-containing compounds, the displacement was explained by charge donation from Ba to electron-deficient Ga, while for Ag, Cu, and Au, the displacement was linked with geometrical reasons.

Material Characterization

XRD measurements showed that mainly type I clathrate phase (no. 223, $Pm3\bar{n}$) with a minor Ge impurity (<2 wt.%) was obtained. The highest amount of Ge was observed for samples with nominal excess of electrons, and the lowest for samples with charge-balanced composition. An example diffraction pattern is shown in Fig. 3. The measured lattice parameters are presented in Fig. 4 as a function of increasing Ga content. In each of the
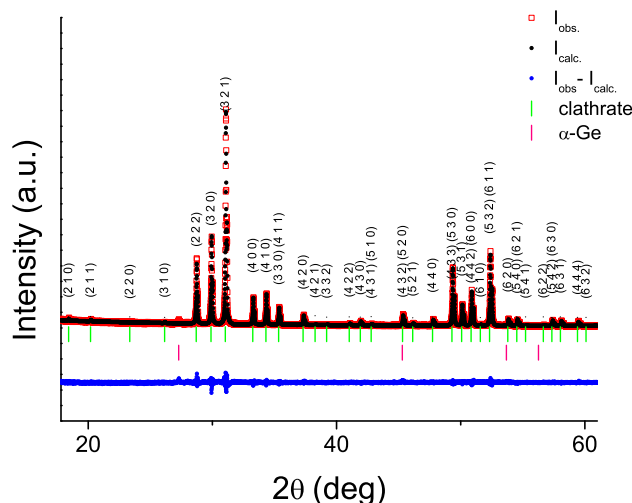

Fig. 3. Example x-ray diffraction pattern for $Ba_8Zn_6Ga_4Ge_{36}$.
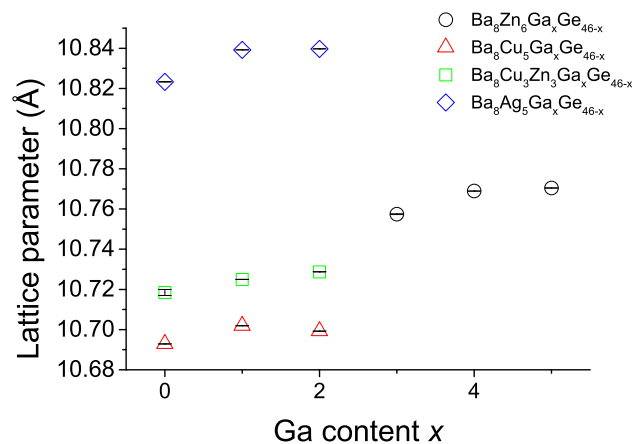

Fig. 4. Lattice constant versus Ga content in $Ba_8TM_xGa_yGe_{46-x-y}$.

prepared series of samples, the lattice parameter is increasing with Ga content for all samples with charge excess (starting from 1 e/u.c.) up to the composition for which complete charge compensation is achieved. This is in agreement with literature results.[4,8,9,11,20–22] The main reason for this dependence is decrease of Ge vacancy concentration. However, it is also possible that the substitution of Ge by Ga, whose atomic radius is greater than that of Ge, could make an important contribution to the increase of the lattice parameter. Further increase of the Ga content changes the lattice parameter very little. For the Zn-, Cu/Zn-, and Ag-containing samples, none or only a tiny cell parameter increase was observed. In literature, similar behavior was observed for most germanium clathrates, being a result of reaching the solubility limit of the substituting elements. On the other hand, in the Cu-containing sample, the lattice parameter decreased with further increase of the Ga content. Similar behavior was already observed for type I germanium clathrates with nominal electron deficiency upon

increase of TM content.[20,27,28] A likely explanation could be that compounds with composition close to complete charge compensation have very low vacancy concentration, which does not affect the cell size, and a difference between the radius of Ge and the substituting element has the main impact on the lattice parameter. The measured lattice parameter values lie between results found in literature for similar compositions. SEM observations (Fig. 5) confirmed that the prepared samples consisted mainly of a phase corresponding to the clathrate composition, but the actual compositions determined by EDS analysis (Table III) showed some deviations from nominal stoichiometry. Germanium clathrates are known to be prone to vacancy creation, and generally for Ba$_8$TM$_x$Ge$_{46-x-y}$□$_y$, it is observed that the vacancy concentration is strongly correlated with the TM concentration. Unfortunately, it was not possible to deduce reliable data for the vacancy concentration in our specimens, due to a high uncertainty of the EDS analysis and very similar x-ray scattering factors for Ge and Ga in Rietveld refinement of PXRD data. An indication of the presence of vacancies may be just the presence of Ge in the prepared samples. In many papers devoted to vacancies in germanium clathrates substituted by TM, i.e., Ba$_8$TM$_{x+y}$Ga$_{43-y}$□$_{3-x}$, Ba$_8$Ga$_{43}$□$_3$ is chosen as a starting composition for a defect model. In such a model, it is assumed that TM fills the vacancies first, then substitutes Ge. This model describes experimental data in only a narrow composition range for low x, close to 0. Let us take as the starting point the completely charge-balanced composition, i.e., Ba$_8$Ga$_{16}$Ge$_{30}$. Employing Kröger–Vink notation, used for description of defects in ionic compounds, it is possible to write defect equations for Ge clathrates. From QTAIM analysis, we know that the net charges of the guest and framework atoms are far from the formal charges. However, as shown in many papers, an electron-counting scheme, where complete charge transfer from guest atoms to a framework is assumed, enables an easy description of the electronic properties and stoichiometry of clathrates:

$$Ba_8Ga_{16}Ge_{30} = Ba_8^{2+}[Ga_{16}^-Ge_{30}]^{16-} = 8Ba_i^{\cdot\cdot} + 16Ga_{Ge}^{'} + 30Ge_{Ge}. \quad (1)$$
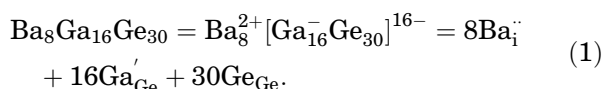
We can understand the negative charge at Ga as an additional charge coming from a Ba electron, occupying an originally empty Ga sp^3 orbital. If we replace one of the Ga by Ge, we have

$$Ba_8Ga_{15}Ge_{31} = 8Ba_i^{\cdot\cdot} + 15Ga_{Ge}^{'} + 31Ge_{Ge} + e^{'}, \quad (2)$$

and one excess electron must appear. The energy of Ga at Ge position is higher than for Ge atom at Ge site, but creation of an extra electron located in the conduction band increases the overall energy, thus it is not energetically favorable. On the other hand, it is thermodynamically possible that in such a compound a vacancy at Ge site can be created:
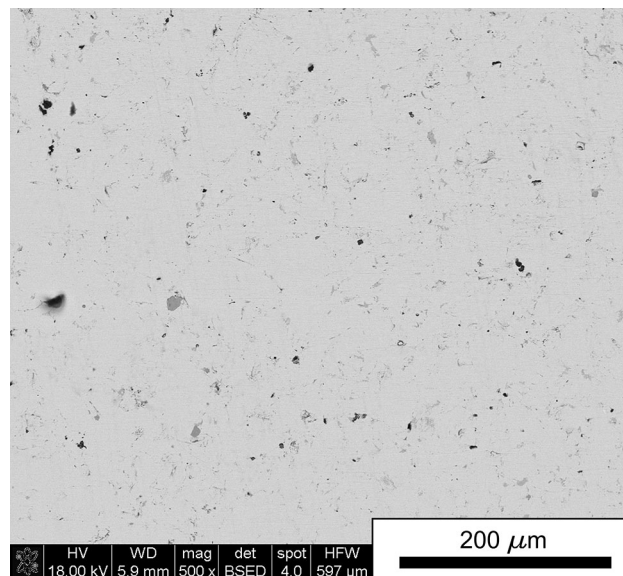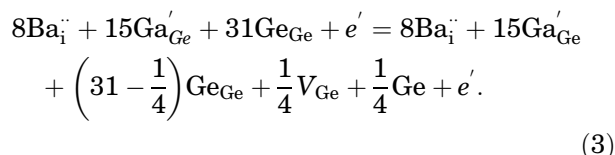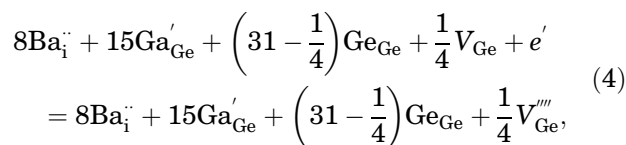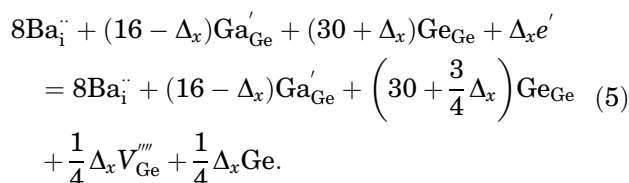

Fig. 5. Example cross-section backscattered electron scanning electron microscopy (BSE-SEM) image of dense, sintered Ba$_8$Ag$_5$Ga$_1$Ge$_{40}$ sample.

$$8Ba_i^{\cdot\cdot} + 15Ga_{Ge}^{'} + 31Ge_{Ge} + e^{'} = 8Ba_i^{\cdot\cdot} + 15Ga_{Ge}^{'}$$
$$+ \left(31 - \frac{1}{4}\right)Ge_{Ge} + \frac{1}{4}V_{Ge} + \frac{1}{4}Ge + e^{'}. \quad (3)$$
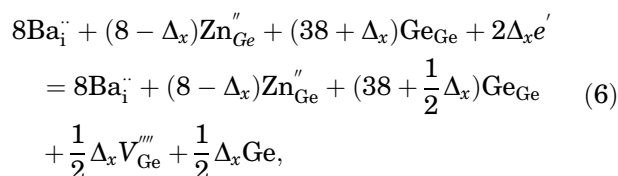
Formation of a vacancy is associated with creation of four dangling bonds, which are nonbonding electrons of four three-bonded Ge atoms surrounding the vacancy. To reduce the overall energy, the excess electrons are trapped by the Ge vacancy V_{Ge} (what in fact is realized by pairing the excess electrons with the dangling bonds):

$$8Ba_i^{\cdot\cdot} + 15Ga_{Ge}^{'} + \left(31 - \frac{1}{4}\right)Ge_{Ge} + \frac{1}{4}V_{Ge} + e^{'}$$
$$= 8Ba_i^{\cdot\cdot} + 15Ga_{Ge}^{'} + \left(31 - \frac{1}{4}\right)Ge_{Ge} + \frac{1}{4}V_{Ge}^{''''}, \quad (4)$$

giving the general equation

$$8Ba_i^{\cdot\cdot} + (16 - \Delta_x)Ga_{Ge}^{'} + (30 + \Delta_x)Ge_{Ge} + \Delta_x e^{'}$$
$$= 8Ba_i^{\cdot\cdot} + (16 - \Delta_x)Ga_{Ge}^{'} + \left(30 + \frac{3}{4}\Delta_x\right)Ge_{Ge} \quad (5)$$
$$+ \frac{1}{4}\Delta_x V_{Ge}^{''''} + \frac{1}{4}\Delta_x Ge.$$

We can create analogous equations for Zn- and Cu/Ag-substituted clathrates:

$$8Ba_i^{\cdot\cdot} + (8 - \Delta_x)Zn_{Ge}^{''} + (38 + \Delta_x)Ge_{Ge} + 2\Delta_x e^{'}$$
$$= 8Ba_i^{\cdot\cdot} + (8 - \Delta_x)Zn_{Ge}^{''} + (38 + \frac{1}{2}\Delta_x)Ge_{Ge} \quad (6)$$
$$+ \frac{1}{2}\Delta_x V_{Ge}^{''''} + \frac{1}{2}\Delta_x Ge,$$

Table III. Selected properties of obtained $Ba_8TM_xGa_yGe_{46-x-y}$ samples: nominal and corresponding composition determined from EDS analysis, measured density, E_g calculated using DFT versus E_g estimated by different methods, and carrier concentration estimated from Mott's formula. Absence of the estimated E_g value means that, for this certain case, the estimation method failed

Excess e^- (f.u.)	Nominal composition	EDS analysis	Density (g/cm³)	Relative density (%)	E_g^{I} (eV)	E_g^{II} (eV)	$E_g^{bipolar}$ (eV)	Estimated carrier concentration, n (10^{21} cm^{-3})
Theoretical E_g for $Ba_8Zn_6Ge_{40}$—0.63 eV								
1	$Ba_8Zn_6Ga_3Ge_{37}$	$Ba_{7.0}Zn_{6.4}Ga_{3.47}Ge_{39.9}$	5.77	98.6	–	–	–	3.1
0	$Ba_8Zn_6Ga_4Ge_{36}$	$Ba_{7.9}Zn_{6.2}Ga_5Ge_{34.9}$	5.67	97.4	–	–	–	7.6
−1	$Ba_8Zn_6Ga_5Ge_{35}$							
Theoretical E_g for $Ba_8Cu_3Zn_3Ge_{40}$—0.44 eV								
1	$Ba_8Zn_3Cu_3Ge_{40}$	$Ba_{8.7}Zn_{3.2}Cu_{1.2}Ga_{1.6}Ge_{38.3}$	5.73	96.8	–	–	–	8.7
0	$Ba_8Zn_3Cu_3Ga_1Ge_{39}$	$Ba_{9.5}Zn_{4.3}Cu_{3.9}Ga_{0.9}Ge_{34.2}$	5.92	99.8	–	–	–	0.53
−1	$Ba_8Zn_3Cu_3Ga_2Ge_{38}$							
Theoretical E_g for $Ba_8Cu_6Ge_{40}$—0.33 eV								
1	$Ba_8Cu_5Ge_{41}$	$Ba_{6.6}Cu_{5.4}Ga_{2.5}Ge_{40.9}$	5.99	99.7	0.32	0.22	0.15	0.43
0	$Ba_8Cu_5Ga_1Ge_{40}$	–	5.83	98.0	–	0.19	–	0.5
−1	$Ba_8Cu_5Ga_2Ge_{39}$							
Theoretical E_g for $Ba_8Ag_6Ge_{40}$—0.16 eV								
1	$Ba_8Ag_5Ge_{41}$	$Ba_{7.65}Ag_{5.73}Ge_{40.59}$	5.93	99.7	–	0.2	–	1.4
0	$Ba_8Ag_5Ga_1Ge_{40}$	$Ba_{7.39}Ag_{5.08}Ga_{1.9}Ge_{40.21}$	5.67	99.0	0.26	0.33	0.3	0.6
−1	$Ba_8Ag_5Ga_2Ge_{39}$							

Theoretical and Experimental Study on Thermoelectric Properties of $Ba_8TM_xGa_yGe_{46-x-y}$ (TM = Zn, Cu, Ag) Type I Clathrates

5273

$$8Ba_i^{..} + \left(\frac{16}{3} - \Delta_x\right)Cu_{Ge}''' + \left(40\frac{2}{3} + \Delta_x\right)Ge_{Ge}$$

$$+ 3\Delta_x e' = 8Ba_i^{..} + \left(\frac{16}{3} - \Delta_x\right)Cu_{Ge}''' \qquad (7)$$

$$+ \left(40\frac{2}{3} + \frac{1}{4}\Delta_x\right)Ge_{Ge} + \frac{3}{4}\Delta_x V_{Ge}'''' + \frac{3}{4}\Delta_x Ge.$$

Using the above equations for the germanium clathrates $Ba_8TM_xGe_{46-x-y}V_{(Ge)y}$, the dependence between the vacancy amount y and the TM amount x and the type of substituting element can be written as

$$y = k \cdot \left(\frac{4}{k} - x\right), \qquad (8)$$

where k is ¼ for Ga or Al, ½ for Zn or Cd, ¾ for Cu or Ag, and 1 for Ni or Pd. In reality, these dependencies are more complicated and lie between the mentioned equation (as an upper limit of the vacancy concentration up to about three vacancies per formula unit, which tends to be the vacancy concentration limit)[22] and a bottom limit with no vacancy. As long as the vacancy formation enthalpy is more energetically expensive than carrier generation, it is possible to increase the electron concentration by decrease of x without a huge increase in the number of vacancies. This situation can occur in germanium clathrates when the deviation from charge balance is low, similarly to the works of Alleno et al.[29] and Zeiringer et al.[24] It is highly probable that synthesis conditions also play a role in creation of vacancies, because in other reports on Zn and Ag germanium clathrates, vacancies were detected in the whole composition range above the charge-balanced composition. Further decrease of x causes increase of the carrier concentration, but with parallel creation of vacancies, where the relation between the TM amount and y is generally close to the formula derived from the defect equations. When y approaches 3, this dependence becomes no longer valid and y tends to 3 as x decreases to 0.

Electronic Properties

All of the prepared samples exhibited negative Seebeck coefficient α over the whole measured temperature range (Fig. 6), pointing to electrons as the majority charge carriers. For most of the samples, the thermopower was almost linearly dependent on temperature, which is characteristic for strongly degenerate semiconductors and metallic systems. The measured electrical conductivity σ is shown in Fig. 7. For the majority of the samples, the conductivity showed metallic-like character and was decreasing with temperature. In the case of samples showing semiconducting character of the temperature dependence, one can observe a corresponding decrease of the absolute value of the
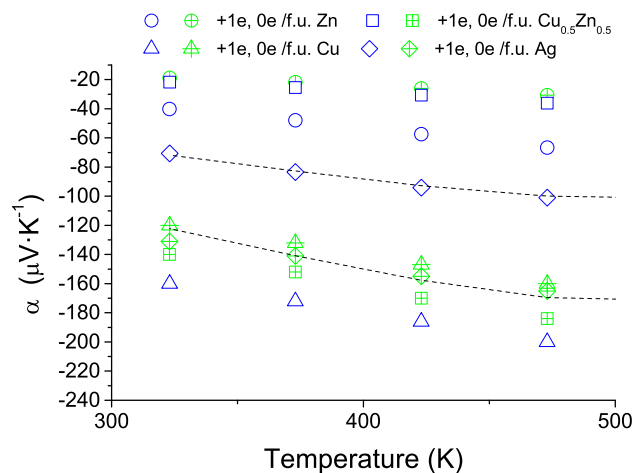

Fig. 6. Temperature dependence of Seebeck coefficient for all samples. Dashed lines are thermopower fits using the model described in the text.
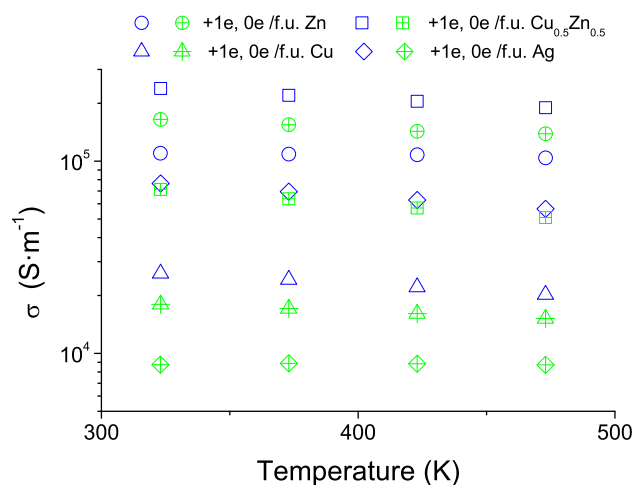

Fig. 7. Temperature dependence of electrical conductivity for all samples.

Seebeck coefficient with temperature, being a result of an increasing contribution of intrinsic carriers. The highest conductivities were found for samples containing Zn and Cu/Zn, with the one exception of $Ba_8Zn_3Cu_3Ge_{40}$. Samples containing Cu and Ag generally had lower conductivities. The observed tendencies of the Seebeck coefficient are linked to those observed for the conductivity. Looking at 320 K, the highest absolute α values are observed for Cu and Ag, and the lowest for samples containing Zn and Cu/Zn. It seems that mainly the charge carrier concentration determines these properties. Comparison of different $Ba_8TM_xGa_{46-x}$ clathrates by Johnsen et al.[30] showed that they have comparable charge carrier mobilities and effective masses, leading to similar thermoelectric power factors $\alpha^2\sigma$. Our observations are compatible with Johnsen et al.'s conclusions. This is in agreement with the results of DFT calculations, showing minor changes

of DOS for clathrate framework substitution with different TM. Using literature values for effective electron masses[4] and Mott's formula, we estimated the charge carrier concentration. As this estimation method uses several approximations, such as a single carrier type with one dominant scattering mechanism, these calculated carrier concentration values should be treated as very approximate. Generally, the lowest absolute values of the Seebeck coefficient are observed for samples with one excess electron per unit cell; these samples also have the highest electrical conductivity, as they should have the highest electron concentration. The charge-balanced samples exhibit the highest absolute values of thermopower, and their electrical conductivity is lower than for the previous group of samples. Because of the difficulties in obtaining a charge carrier concentration adequate for the stoichiometry, the general description of our observations has of course several exceptions. The discrepancy between the nominal composition and the electronic properties is a known issue in Ge clathrates.[31] In the case of Ni-containing clathrate, Johnsen et al.[30] suggested formation of vacancies as a possible explanation for this disagreement, and this seems to be a reasonable explanation for the variations observed in our samples as well.

To evaluate the band-structure calculations we made an attempt to compare the calculated and experimental bandgap energy E_g. For most of the samples, the thermopower and electrical conductivity changed monotonically with temperature without inflection or critical points, which reflects the rising contribution of intrinsic carriers. The absence of such features impedes the use of the typical E_g estimation method from Arrhenius plots. First, we tried to use resistivity data to estimate E_g in a manner similar to one used by Melnychenko-Koby-luk et al.,[8] but the obtained gap values were close to 1 eV or higher, appearing to be overestimated. To evaluate the energy gap experimentally, we used two methods: (i) a method proposed by Goldsmid and Sharp[32] based on the maximum in the $\alpha(T)$ dependence, (ii) a fit of a semiempirical formula to the $\alpha(T)$ dependence. The first method is applicable only in the case of having a maximum in the $\alpha(T)$ dependence and uses the formula

$$\alpha_{\max} = \frac{E_g}{2e \cdot T_{\max}}, \qquad (9)$$

where $\alpha_{\max}$ is the maximum value of the absolute Seebeck coefficient, E_g is the energy gap, e is the electron charge, and $T_{\max}$ is the temperature of the Seebeck coefficient maximum. In the second approach, we used the fact that, for degenerate semiconductors, the Seebeck coefficient increases almost linearly with temperature as $\alpha(T) \approx a \cdot T$, where a is a slope coefficient. This kind of temperature dependence is usually observed in germanium clathrates.[8,24] While taking into account minority

carriers, the Seebeck coefficient is proportional to a term

$$\alpha \sim \frac{n_e \cdot \mu_e - n_h \cdot \mu_h}{n_e \cdot \mu_e + n_h \cdot \mu_h}, \qquad (10)$$

where n_e and n_h are the electron and hole concentrations, and μ_e and μ_h are the electron and hole mobility, respectively. The fitting function used was

$$\alpha(n_e, \mu_e, n_h, \mu_h, E_g, T) = a$$
$$\cdot T \left[\frac{n_e(E_g, T) \cdot \mu_e - n_h(E_g, T) \cdot \mu_h}{n_e(E_g, T) \cdot \mu_e + n_h(E_g, T) \cdot \mu_h} \right], \qquad (11)$$

assuming a constant mobility of electrons and holes. Results of these estimations are presented in Table III, and examples of the obtained fits for $\alpha(T)$ are included in Fig. 6. Equations used in the second method were least-square fits to the experimental data using Levenberg–Marquardt and quasi-Newton methods. The estimated bandgap values derived from the other two methods gave satisfactory correlation with those calculated theoretically, showing decreasing bandgap energy when changing TM from Zn through Cu to Ag. Our estimations are comparable to findings of other researchers presented in Table IV. Obviously, these estimates strongly depend on the selected method, as for most of them several approximations and simplifications are applied. Nevertheless, they give some qualitative information on how the energy gap is influenced by TM substitution, which is useful for designing better thermoelectric materials. The accuracy and applicability of these methods should be increased for measurements at higher temperature ranges. The estimated energy gaps reflect trends observed in theoretical calculations, where the calculated gaps are decreasing from Ga through Zn samples and are lowest for Cu and Ag samples. Although for $Ba_8Zn_xGa_xGe_{46-x-y}$ and $Ba_8Zn_{3-x/2}Cu_{3-x/2}Ga_yGe_{46-x-y}$ we could not estimate the energy gaps due to the absence of any features in the $\alpha(T)$ dependence, for the same reason we suspect these specimens have energy gaps higher than for Cu and Ag samples. This observation is also supported by literature data (Table IV). It is important to notice that the variability of the estimated E_g values for similar compositions is large. Moreover, the application of different estimation methods for one sample gives very different results.[24]

Thermal Conductivity

The results of the total thermal conductivity measurements are presented in Fig. 8. The inset in Fig. 8 shows the lattice thermal conductivity calculated using the electrical conductivity and the Wiedemann–Franz law for estimation of the electronic contribution to the total thermal conductivity. Depending on the electrical conductivity of the sample, the calculated contribution of the electronic thermal conductivity to the total thermal

Theoretical and Experimental Study on Thermoelectric Properties of $Ba_8TM_xGa_yGe_{46-x-y}$
(TM = Zn, Cu, Ag) Type I Clathrates

5275

Table IV. Bandgap energy E_g values reported in Ba–TM–Ge type I clathrates

Composition	E_g (eV)	Estimation method
$Ba_8Zn_{2.1}Ge_{41.5}\square_{2.4}$[8]	0.49	Reflectance measurement
$Ba_8Zn_{4.6}Ge_{40.0}\square_{1.4}$[8]	0.48	Reflectance measurement
$Ba_8Zn_{5.7}Ge_{40.0}\square_{0.3}$[8]	0.45	Reflectance measurement
$Ba_8Zn_{7.7}Ge_{38.3}$[8]	0.73	Reflectance measurement
$Ba_8Zn_{2.1}Ge_{41.5}\square_{2.4}$[8]	0.14	Resistivity fit
$Ba_8Zn_8Ge_{38}$[34]	0.4	Goldsmid and Sharp
$Ba_8Zn_xGa_yGe_{46-x-y}$[34]	0.3–0.5	Goldsmid and Sharp
$Ba_8Cu_{5.33}Ge_{40.67}$[34]	0.1	Goldsmid and Sharp
$Ba_8Ag_{4.1}Ge_{41.4}\square_{0.5}$[24]	0.72	Resistivity fit
$Ba_8Ag_{4.8}Ge_{41.2}$[24]	0.6	Resistivity fit
$Ba_8Ag_{4.1}Ge_{41.4}\square_{0.5}$[24]	0.34	Goldsmid and Sharp
$Ba_8Ag_{4.8}Ge_{41.2}$[24]	0.29	Goldsmid and Sharp
$Ba_8Ge_{43}\square_3$[22]	0.06	Arrhenius equation
$Ba_8Ga_{16}Ge_{30}$[35]	0.5	Arrhenius equation
[36]	0.4	Goldsmid and Sharp
[37]	0.3	Goldsmid and Sharp
[38]	0.39	Goldsmid and Sharp
[38]	0.41	Arrhenius equation
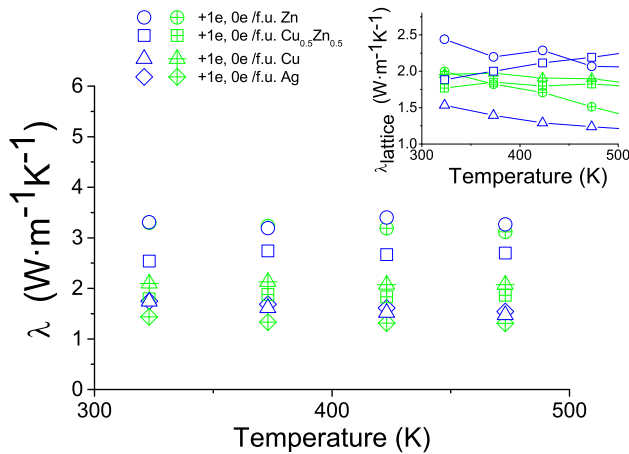
Fig. 8. Thermal conductivity versus temperature for Zn, Cu, and Cu/Zn $Ba_8TM_xGa_yGe_{46-x-y}$ samples. The inset shows the calculated lattice thermal conductivity.

conductivity varies from a few percent up to almost 30%. For most of the Zn-, Cu-, and Cu/Zn-containing samples, the thermal conductivity is decreasing with temperature from 320 K up to 720 K, whereas for Ag-containing samples, the thermal conductivity decreases with temperature, then reaches a minimum and increases to values even higher than at 320 K. Taking into account the electronic transport properties of the Ba–Ag–Ga–Ge clathrates, this particular behavior can be explained by the bipolar thermal conductivity mechanism. This is a result of different generation and recombination rates of electron–hole pairs in the cold and hot part of a semiconductor and arises when both electrons and holes contribute to the electrical conductivity. This mechanism can be included in the Wiedemann–Franz law $\lambda_{el} = L \cdot \sigma \cdot T$ by the introduction of a

modified Lorenz number L, which can be written for a semiconductor with dominant alloy scattering as

$$L = \left(\frac{k_B}{e}\right)^2 \cdot \left[2 + \left(4 + \frac{E_g}{k_B T}\right)^2 \frac{\sigma_e \cdot \sigma_h}{\sigma_{total}^2}\right], \quad (12)$$

where k_B is the Boltzmann constant, e is the elementary charge, and σ_e, σ_h, and σ_{total} are the electron, hole, and total electrical conductivity, respectively. We performed a fit of the thermal conductivity of Ag-containing samples using the modified Lorenz number and the experimental values of electrical conductivity. The electron and hole conductivities were derived using the functions

$$\sigma_e(T) = e \cdot \mu(T) \cdot n_e(T) \quad (13)$$

and

$$\sigma_h(T) = e \cdot \mu(T) \cdot n_h(T), \quad (14)$$

assuming that the carrier mobility μ can be described in the studied temperature region by

$$\mu(T) = \mu_0(T) + c \cdot T^r \quad (15)$$

and the charge carrier concentration temperature dependence is

$$n_e(T) = n_0 + c' \cdot \exp\left(\frac{-E_g}{kT}\right) \quad (16)$$

for electrons and

$$n_h(T) = c' \cdot \exp\left(\frac{-E_g}{kT}\right) \quad (17)$$

for holes. c and c' are numerical constants fit during the data fitting procedure, and e is the electron charge. In Eq. 15, we used an exponent $r = -1/2$, as in several papers[31,33] it was shown for germanium clathrates that, at temperatures above 100 K, the
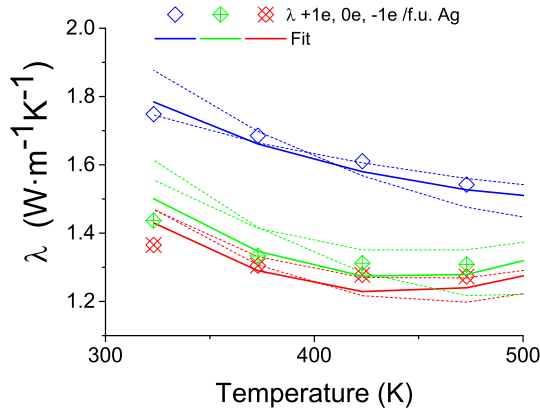
Fig. 9. Thermal conductivity for $Ba_8Ag_5Ga_yGe_{41-y}$ samples.

Fig. 10. Thermoelectric figure of merit ZT as a function of temperature for $Ba_8TM_xGa_yGe_{46-x-y}$ samples.

Hall mobility shows alloy scattering behavior where $\mu(T) \sim T^{-1/2}$. It was also assumed that the dominant phonon scattering mechanism is the Umklapp process, and the lattice component of the thermal conductivity is proportional to T^{-1}. The results are shown in Fig. 9 together with curves calculated for a higher and lower E_g value than the one giving the best fit, having sum of squared error twice as high as for the best fit. The proposed model can describe the total conductivity quite well, providing support to the assumption of bipolar thermal conductivity in the Ag-containing samples. Moreover, the E_g values from the fits are quite reasonable compared with the other estimations. The lowest thermal conductivity is observed in Ag clathrate samples. This can be explained by the enhanced phonon alloy scattering on Ag atoms. The atomic mass of silver is much higher than those of Cu, Zn, Ga, and Ge, thus the mass fluctuations in the crystal lattice are higher and for the same degree of disorder the phonon scattering is more effective. The Zn, Cu, and Cu/Zn clathrates have thermal conductivity lying in a very similar range, but the Zn specimens have slightly higher average conductivity. Because the atomic mass differences between Cu, Zn, Ga, and Ge are small, introduction of a greater number of elements into the clathrate structure has little impact on the thermal conductivity.

Using the Seebeck coefficient as well as electrical and thermal conductivity results, the thermoelectric figure of merit ZT was calculated (Fig. 10). The highest value of $ZT = 0.45$ is reached at 670 K for $Ba_8Ag_5Ge_{41}$. In most cases, except the Cu/Zn sample, the best thermoelectric performance in each series of samples is shown by the sample with the nominal excess electron per f.u. Nevertheless, they are far from the optimized carrier concentration. The Zn and Cu/Zn samples have too high carrier concentration, contrary to Cu and Ag samples, which have a low concentration. It can be expected that careful stoichiometry change would result in thermoelectric performance improvement. For the two best materials—$Ba_8Ag_5Ge_{41}$ and

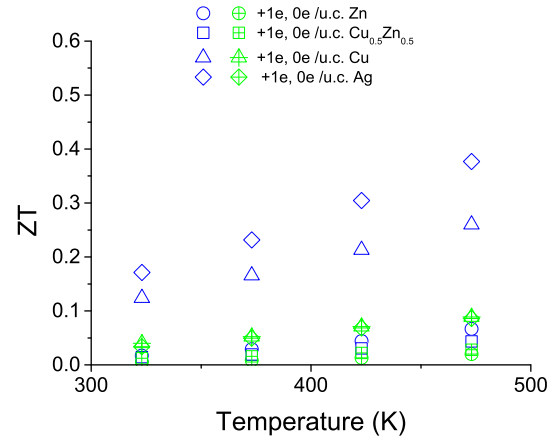$Ba_8Cu_5Ge_{41}$—this improvement seems to be limited by the high minority carrier concentration. This is a consequence of the relatively narrow energy bandgap of these Ba–TM–Ge clathrates. More prospective are the Zn–Ge or Ga–Ge clathrates combined with TM, having atomic masses significantly higher than Ge and Zn, which would have lower concentration of minority carriers at high temperatures and simultaneously possess the advantage of higher phonon scattering rate. Band-structure calculations should be helpful to determine combinations of Ge-substituting elements such that the lattice disorder and mass fluctuations are maximized while decreasing the bandgap energy as little as possible.

CONCLUSIONS

Systematic band-structure calculations showed that the total density of states remains almost unchanged for different elements substituting at 6*c* site in type I $Ba_8TM_6Ge_{40}$ clathrates. However, significant DOS modifications are possible on substitution at different atomic sites. More detailed band-structure analysis showed that, for Zn, $Cu_{1/2}Zn_{1/2}$, Cu, and Ag, the contribution of *d*-orbitals to the density of states increases, modifying the shape of the partial DOS of the 6*c* site atom. With increasing *d*-character of the conductivity and valence bands, the width of the energy gap is decreasing. The calculated bandgap values are quite coherent with estimations based on measured Seebeck coefficient temperature dependence. Theoretical lattice parameters are also in good agreement with experimental data. QTAIM analysis points out the correlation of the topological charge of TM atom and electronegativity difference between Ge and TM. The atomic charge of Ga and Zn is positive, while for Cu and Ag it is negative, which can impact on TM interactions with guest cation and on structural stability.

The electrical resistivity of prepared type I germanium clathrate $Ba_8TM_xGa_yGe_{46-x-y}$ samples showed mainly metallic-like character. All samples

had negative Seebeck coefficient ranging between -25 μV/K and -160 μV/K at 320 K. Dopant type had much less effect on transport properties than the carrier concentration. The lowest thermal conductivity was observed for Ag-substituted samples. The increase of the thermal conductivity with temperature for Ag samples at higher temperatures can be successfully described by the bipolar conductivity mechanism. The highest $ZT_{max} = 0.45$ at 670 K was observed for the nominal composition $Ba_8Ag_5Ge_{41}$. For Ag and Cu samples, the thermoelectric performance is very promising, and relatively high ZT values are reached at lower temperature than for other Ge clathrates. Unfortunately, ZT_{max} is limited by increasing minority carrier contribution. Taking this into account, it should be possible to obtain the highest thermoelectric performance in clathrates with wider energy gap. Electrical properties of the obtained samples are strongly dependent on vacancy formation as it changes the carrier concentration. We propose defect equations to describe vacancy formation in the type I Ge clathrates in the compositional region close to charge balance toward excess electrons. Strong deviation from the charge-balanced composition produces Ge site vacancies and thus deteriorates the thermoelectric properties of the material by closing the energy gap and reducing the electron mobility..

ACKNOWLEDGEMENTS

OPEN ACCESS

ELECTRONIC SUPPLEMENTARY MATERIAL

The online version of this article (doi:10.1007/s11664-016-4669-0) contains supplementary material, which is available to authorized users.

REFERENCES

1. B.C. Sales, D. Mandrus, and B.C. Chakoumakos, *Semiconduct. Semimet.* 70, 1 (2001).
2. G.S. Nolas, G.A. Slack, and S.B. Schujman, *Semiconduct. Semimet.* 69, 255 (2001).
3. G.S. Nolas, J.L. Cohn, G.A. Slack, and S.B. Schujman, *Appl. Phys. Lett.* 73, 178 (1998).
4. M. Christensen, S. Johnsen, and B.B. Iversen, *Dalton Trans.* 39, 978 (2010).
5. T. Takabatake, K. Suekuni, T. Nakayama, and E. Kaneshita, *Rev. Mod. Phys.* 86, 669 (2014).
6. K. Momma and F. Izumi, *J. Appl. Crystallogr.* 44, 1272 (2011).
7. G. Cordier and P. Woll, *J. Less Common Met.* 169, 291 (1991).
8. N. Melnychenko-Koblyuk, A. Grytsiv, L. Fornasari, H. Kaldarar, H. Michor, F.R. Röhrbacher, M. Koza, E. Royanian, E. Bauer, P. Rogl, M. Rotter, H. Schmid, F. Marabelli, A. Devishvili, M. Doerr, and G. Giester, *J. Phys. Condens. Matter.* 19, 216223 (2007).
9. T. Eto, K. Kishimoto, K. Koga, K. Akai, T. Koyanagi, H. Anno, T. Tanaka, H. Kurisu, S. Yamamoto, and M. Matsuura, *Mater. Trans.* 50, 631 (2009).
10. N.A. Borshch, N.S. Pereslavtseva, and S.I. Kurganskii, *Semiconductors* 43, 563 (2009).
11. J.H. Chen, A.S. Arvij, X. Zheng, S.Y. Rodriguez, and J.H. Ross Jr, *J. Alloy. Compd.* 593, 261 (2014).
12. P. Blaha, K. Schwarz, G.K.H. Madsen, D. Kvasnicka, and J. Luitz, *WIEN2k, An Augmented Plane Wave + Local Orbitals Program for Calculating Crystal Properties* (Wien: Karlheinz Schwarz, Techn. Universität Wien, 2001).
13. T.L. Loucks, *Augmented Plane Wave Method* (New York: Benjamin, 1967).
14. O.K. Andersen, *Solid State Commun.* 13, 133 (1973).
15. D.R. Hamann, *Phys. Rev. Lett.* 42, 662 (1979).
16. E. Wimmer, H. Krakauer, M. Weinert, and A.J. Freeman, *Phys. Rev. B* 24, 864 (1981).
17. D.J. Singh, *Planewaves, Pseudopotentials and the LAPW Method* (Dordrecht: Kluwer Academic, 1994).
18. F. Tran and P. Blaha, *Phys. Rev. Lett.* 102, 226401 (2009).
19. J. Leszczynski, A. Kolezynski, and K.T. Wojciechowski, *J. Solid State Chem.* 193, 114 (2012).
20. S. Johnsen, A. Bentien, G.K.H. Madsen, B.B. Iversen, and M. Nygren, *Chem. Mater.* 18, 4633 (2006).
21. S. Johnsen, M. Christensen, B. Thomsen, G.K.H. Madsen, and B.B. Iversen, *Phys. Rev. B* 82, 184303 (2010).
22. U. Aydemir, C. Candolfi, H. Borrmann, M. Baitinger, A. Ormeci, W. Carrillo-Cabrera, C. Chubilleau, B. Lenoir, A. Dauscher, N. Oeschler, F. Steglica, and Yu Grin, *Dalton Trans.* 39, 1078 (2010).
23. Y. Li, J. Chi, W. Gou, S. Khandekar, and J.H. Ross Jr, *J. Phys. Condens. Matter.* 15, 5535 (2003).
24. I. Zeiringer, M.X. Chen, I. Bednar, E. Royanian, E. Bauer, R. Podloucky, A. Grytsiv, P. Rogl, and H. Effenberger, *Acta Mater.* 59, 2368 (2011).
25. M. Baitinger, B. Böhme, A. Ormeci, and Y. Grin, *Physics and Chemistry of Inorganic Clathrates* (Dordrecht: Springer, 2014), pp. 35–64.
26. H. Zhang, H. Borrmann, N. Oeschler, C. Candolfi, W. Schnelle, M. Schmidt, U. Burkhardt, M. Baitinger, J.T. Zhao, and Y. Grin, *Inorg. Chem.* 50, 1250 (2011).
27. N. Melnychenko-Koblyuk, A. Grytsiv, P. Rogl, H. Schmid, and G. Giester, *J. Solid State Chem.* 182, 1754 (2009).
28. H. Zhang, J.T. Zhao, M.B. Tang, Z.Y. Man, H.H. Chen, and X.X. Yang, *J. Alloy. Compd.* 476, 1 (2009).
29. E. Alleno, G. Maillet, O. Rouleau, E. Leroy, C. Godart, W. Carrillo-Cabrera, P. Simon, and Y. Grin, *Chem. Mater.* 21, 1485 (2009).
30. S. Johnsen, A. Bentien, G.K.H. Madsen, M. Nygren, and B.B. Iversen, *Phys. Rev. B* 76, 245126 (2007).
31. M. Hokazono, H. Anno, and K. Matsubara, *Mater. Trans.* 46, 1485 (2005).
32. H.J. Goldsmid and J.W. Sharp, *J. Electron. Mater.* 28, 869 (1999).
33. M. Falmbigl, N. Nasir, A. Grytsiv, P. Rogl, S. Seichter, A. Zavarsky, E. Royanian, and E. Bauer, *J. Phys. D* 45, 215308 (2012).
34. X. Shi, J. Yang, S. Bai, J. Yang, H. Wang, M. Chi, J.R. Salvador, W. Zhang, L. Chen, and W. Wong, *Adv. Funct. Mater.* 20, 755 (2010).

35. T. Matsui, J. Furukawa, K. Tsukamoto, H. Tsuda, and K. Morii, *J. Alloy. Compd.* 391, 284 (2005).
36. D. Cederkrantz, A. Saramat, G.J. Snyder, and A.E.C. Palmqvist, *J. Appl. Phys.* 106, 074509 (2009).
37. E.S. Toberer, M. Christensen, B.B. Iversen, and G.J. Snyder, *Phys. Rev. B* 77, 075203 (2008).
38. A.F. May, E.S. Toberer, A. Saramat, and G.J. Snyder, *Phys. Rev. B* 80, 125205 (2009).